Proceedings of the 2006 American Control Conference
Minneapolis, Minnesota, USA, June 14-16, 2006

Kalman Filtering for Real-Time Individual Cylinder Air Fuel Ratio Observer on a Diesel Engine Test Bench

Jonathan Chauvin, Philippe Moulin, Gilles Corde, Nicolas Petit and Pierre Rouchon

***Abstract*— We propose an estimator of the individual cylinder air fuel ratios in a turbocharged Diesel Engine using as only sensor the single air fuel ratio sensor placed downstream the turbine. The observer consists of a time-varying Kalman Filter based on a physics-based model for the engine dynamics. We prove that the reference system converges toward a limit cycle. This limit cycle is used for the design of an extended Kalman filter. Performance is evaluated through test bench experiments on a 4 cylinder Diesel engine. The proposed approach has the advantage over existing methods of providing insight into the cylinders unbalance by considering a higher frequency model of the exhaust manifold. This information could pave the road to efficient closed loop control strategy as demonstrated on an experimental example.**

I. Introduction

As the performance and environmental requirements have continued to rise over the years, the interest in advances control strategies for automotive applications has increased. In this context, controlling the combustion represents a key challenge being examined by numerous research teams [1], [2] and references therein. Among many, several tentative solutions are combustion torque control and estimation (see for example [3], [4], [5] and [6]), Air Fuel Ratio control and estimation (see [7], [8] and [9]),.... The control of the *individual* Air Fuel Ratio (AFR: the weight ratio of air-to-gasoline), which is a good representation of the torque balance of the engine, has emerged as an important step.

Classically, in spark ignition engines, overall AFR is directly controlled with the injection system. By this control strategy, all cylinders share the same closed-loop input signal based on the single λ-sensor, an oxygen sensor in the exhaust manifold $\lambda \triangleq 1 - \frac{M_{air}}{M_T}$ providing, under lean operating conditions, a direct reading of the normalized Fuel Air Ratio (FAR) measurement [10, chap. 3], and thus of the AFR. Ideally, all the cylinders should have the same AFR as they have the same injection set-point. Unfortunately, due to inherent flaws of the injection system (such as pressure waves and mechanical tolerances), the total mass of fuel injected in each cylinder is very difficult to predict with a relative precision below 7%. This lack of precision results in non optimal engine operating conditions. Consider now a class of planned Homogeneous Charge Compression Ignition (HCCI) engines, referring to [11], [12], [13], [14] for an overview of the technology, [15], [16], [17] for more control oriented models, and [18], [19], [20], [21], [22] for control techniques. For these engines and regeneration filters (Particulate filters, $DeNO_x$ [23], [24], [25], even slight unbalance between the cylinders can in particular induce malicious noise, possible stall and increased emissions. Cylinder-individual control is needed to address the potential drawbacks in these planned technologies. In this context, *cylinder-individual* AFR estimation may provide crucial information to assist the HCCI engine controller. This is the focus of the paper.

In previous published works (see [26] and [27]), the methods used to reconstruct the AFR of each cylinder from the UEGO (Universal Exhaust Gas Oxygen) sensor measurement are based on the permutation dynamics at the TDC (Top-Dead Center) sample angle and a gain identification technique. The requirement we perceive as being critical for efficient control strategies is a high frequency estimation of the individual cylinder AFR: 6^o sample angle estimation instead of 90^o (TDC). We design an observer on the balance model of the exhaust manifold. We use a physics-based model underlying the role of periodic input flows (gas flows from the cylinders into the exhaust manifold).

The contribution of this paper is the design and experimental validation of a real-time high frequency observer based on an extended Kalman filter. Tests are conducted on a four cylinder turbocharged diesel test bench presented in [28]. We stress that this observer is relevant for application purposes by illustrative torque balancing closed loop results.

The paper is organized as follows. In Section II, we present the physics-based model of the exhaust manifold. We prove that the continuous-time dynamics converges toward a limit cycle (x_{per}). In Section III, using this limit cycle, we derive a periodic linear discrete-time model that serves as a reference for a proposed Kalman filter. This discrete-time model is a discrete approximation of continuous-time dynamics by an Euler explicit scheme around the limit cycle x_{per}. Implementation and experimental results are reported in Section IV. Finally, future directions are given in Section V.

II. Exhaust Manifold Model

Figure 1 depicts the flow sheet of the individual AFR from the cylinders outlet down to the turbine, where the sensor is located at. From the cylinders to the AFR sensor (located downstream the turbine) the gases travel through the exhaust pipes, the exhaust manifold and the turbocharger.

J. Chauvin (corresponding author) is a PhD Candidate in Mathematics and Control, Centre Automatique et Systèmes, École des Mines de Paris, 60, bd St Michel, 75272 Paris, France chauvin@cas.ensmp.fr

P. Moulin and G. Corde are with the Department of Engine Control in Institut Français du Pétrole, 1 et 4 Avenue de Bois Préau, 92852 Rueil Malmaison, France

N. Petit and P. Rouchon are with the Centre Automatique et Systèmes, École des Mines de Paris, 60, bd St Michel, 75272 Paris, France

1-4244-0210-7/06/$20.00 ©2006 IEEE

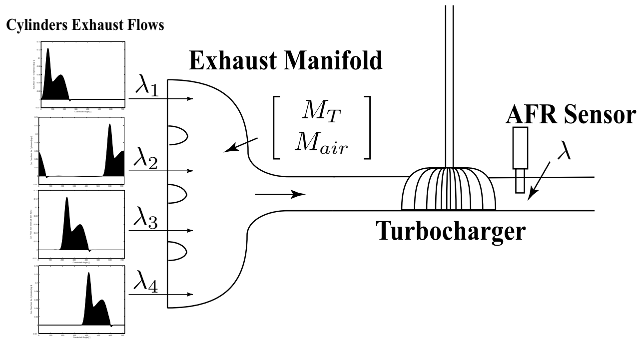

Fig. 1. Individual Air-Fuel Ratio problem: a single sensor located downstream the turbine is available to reconstruct individual AFR.

The AFR can be rewritten, neglecting EGR, as

$$\lambda \triangleq 1 - \frac{M_{air}}{M_T}$$

The various AFR have an influence on the gas pressure, temperature, and composition in the exhaust manifold. In a very naive model, the gases move at constant speed, without mixing. In practice, diffusion and mixing effects are present. Therefore, we propose a nonlinear model to take these into account. Our approach focuses on macroscopic balances involving experimentally derived nonlinear functions.

A. Mass balance in the exhaust manifold

Balance equations are described by (1) and (2). We assume that the individual AFR are constant about a given setpoint. The sensor dynamics is represented as a first order dynamics (3)

$$N_e \frac{dM_T}{d\alpha} = \sum_{i=1}^{n_{cyl}} d_i(\alpha, \Xi) - d_T(M_T, \Xi) \qquad (1)$$

$$N_e \frac{dM_{air}}{d\alpha} = \sum_{i=1}^{n_{cyl}} (1-\lambda_i) d_i(\alpha, \Xi) - \frac{M_{air}}{M_T} d_T(M_T, \Xi) \qquad (2)$$

$$N_e \frac{d\lambda_{mes}}{d\alpha} = \frac{1}{\tau}\left(\frac{M_T - M_{air}}{M_T} - \lambda_{mes}\right) \qquad (3)$$

$$N_e \frac{d\lambda_i}{d\alpha} = 0, \quad \forall i \in [\ 1,\ n_{cyl}\ ] \qquad (4)$$

Notations are given in Table I. Operating conditions are defined by the Ξ parameters (mean aspirated flow D_{asp}, exhaust temperature T_{exh}, turbocharger speed N_{turbo}). They are considered constant over an engine cycle.

The T_0-periodic $d_i(., \Xi)$ functions are modelled through interpolation of a large number of available data. The functions family $\{d_i\}_{i=1 \ldots n_{cyl}}$ is a linearly independent family of the set of continuous T_0-periodic functions.

The flow rate through the turbine d_T is a function of the total mass M_T, smooth away from 0, and can be factorized as

$$d_T(M_T, \Xi) = p(M_T, \Xi) M_T$$

where p is a positive increasing (concave) function with respect to the total mass M_T, e.g. $p(z, \Xi) = p_0(\Xi)\sqrt{2\frac{\gamma}{\gamma-1}((\frac{z}{z_0})^{-\frac{2}{\gamma}} - (\frac{z}{z_0})^{-\frac{\gamma+1}{\gamma}})}$. Usually given by a 2D look up table, the flow rate is modelled as a flow through a restriction, as in [10], whose section depends on the pressure ratio and the turbocharger speed (as proposed in [29] and [30]). Composition of the flow through the turbine and in the exhaust manifold are considered equal.

TABLE I

NOMENCLATURE.

Symb.	Quantity	Unit
α	Crankshaft angle	
M_T	Total mass of gas in the exhaust manifold	kg
M_{air}	Mass of air in the exhaust manifold	kg
N_e	Engine Speed	rpm
d_T	Gas flow rate through the exhaust manifold	kg.s^{-1}
d_i	Gas flow rate from cylinder i	kg.s^{-1}
Ξ	Operating conditions	
D_{asp}	Mean aspirated flow	kg.s^{-1}
T_{exh}	Temperature in the exhaust manifold	^{o}K
N_{turbo}	Turbocharger speed	rpm
r	EGR rate	
λ_i	Normalized Fuel-Air Ratio of cylinder i	
λ	Oxygen sensor measurement	
P	Pressure in the exhaust manifold	bar
z_0	Total mass in the exhaust manifold under atmospherical conditions	kg
n_{cyl}	Number of cylinders	
$\lambda_{i,ref}$	Reference normalized Fuel-Air Ratio of cylinder i	
$\Delta\alpha \triangleq \frac{\pi}{30}$	Angular sample time	
$T_0 \triangleq 4\pi$	Period of the continuous-time dynamics	
$N_0 \triangleq 120$	Period of the discrete-time dynamics	
$\delta \triangleq \frac{\Delta\alpha}{N_e}$	Constant	rpm^{-1}

The measurements are

- P the pressure in the exhaust manifold assumed to be related to the total mass by $P = \gamma_T M_T$ with $\gamma_T \triangleq \frac{RT_{exh}}{V_{exh}}$ considered as a constant over an engine cycle.
- λ_{mes} the Air Fuel Ratio measurement.

B. The masses dynamics converge toward a limit cycle

First, we prove that the exhaust dynamics are a periodically driven contracting system. Then, the Kalman filter is defined in the vicinity of the limit cycle. Total and air masses balance equations (1) and (2) can be written under the form

$$\frac{dM}{d\alpha} = g(\alpha) - f_{\Xi}(M) \qquad (5)$$

where $M = [\ M_T \quad M_{air}\ ]^T$, $f_{\Xi}(M) = \frac{1}{N_e}[\ M_T p(M_T, \Xi) \quad M_{air} p(M_T)\ ]^T$ and $g(\alpha) = \frac{1}{N_e}\sum_{i=1}^{n_{cyl}} d_i(\alpha, \Xi)[\ 1 \quad (1-\lambda_i)\ ]^T$. Let $D \triangleq \{(M_T, M_{air}) \in (\mathbb{R}^+)^2 \ M_T \geq M_{air}$ and $M_T > (1+\epsilon)M_0 \ \ \epsilon > 0\}$. For all $(M_T, M_{air}) \in D$,

$$\begin{aligned} N_e \tfrac{d(M_T - M_{air})}{d\alpha} &= (M_T - M_{air}) p(M_T, \Xi) \\ &\quad + \textstyle\sum_{i=1}^{n_{cyl}} \lambda_i d_i(\alpha, \Xi) \\ &\geq 0 \end{aligned}$$

and $\frac{dM_T}{d\alpha} \geq 0$ because, $\forall \alpha$, $\sum_{i=1}^{n_{cyl}} d_i(\alpha, \Xi) > (1+\epsilon)M_0 p((1+\epsilon)M_0, \Xi)$. It follows that D is positively invariant by the exhaust dynamics (5). The symmetric part of the Jacobian of f is

$$J^+_{f_\Xi}(M) = \frac{1}{N_e} \begin{bmatrix} p(M_T,\Xi) + M_T p'(M_T,\Xi) & \frac{1}{2}M_{air}p'(M_T,\Xi) \\ \frac{1}{2}M_{air}p'(M_T,\Xi) & p(M_T) \end{bmatrix}$$

Computation of its eigenvalues leads to

$$\begin{aligned} \text{eig}(J^+_{f_\Xi}(M)) &= \frac{1}{N_\varsigma}\{p(M_T,\Xi) \\ &+\frac{1}{2}p'(M_T,\Xi)(M_T \pm \sqrt{M_T^2+M_{air}^2})\} \end{aligned}$$

For all $(M_T, M_{air}) \in D$,

$$\frac{1-\sqrt{2}}{2}M_T \leq M_T - \sqrt{M_T^2+M_{air}^2} \leq 0$$

p is increasing,

$$D \ni M \mapsto p(M_T,\Xi) + \frac{1}{2}\dot{p}(M_T,\Xi)(M_T + \frac{1-\sqrt{2}}{2}M_T)$$

is a strictly positive increasing function. Thus,

$$\exists J_0 \in \mathbb{R}^+ \setminus \{0\}, \quad \text{s.t.} \quad \forall M \in D, \quad J^+_{f_\Xi}(M) \geq J_0 I$$

We note $\phi(\alpha, \alpha_0, M_0)$ the trajectory of system (5) at time α with initial condition $\phi(\alpha_0, \alpha_0, M_0) = M_0$, and define the Poincaré map

$$P_{\alpha_0} : D \ni M_0 \mapsto \phi(\alpha_0 + T_0, \alpha_0, M_0) \in D$$

From [31], [32], strict positiveness of J^+_f leads to the contracting property of P_{α_0}, i.e.

$$\begin{aligned} &\forall (M_1, M_2) \in D, \\ &\|P_{\alpha_0}(M_1) - P_{\alpha_0}(M_2)\| \quad \leq \quad e^{-J_0T_0}\|M_1 - M_2\| \end{aligned}$$

Then, from the global inversion theorem, P_{α_0} has a unique fixed point, $\bar{\phi}(\alpha_0)$ and

$$\forall (t_0, M_0) \in \mathbb{R}^+ \times D, \qquad \lim_{k\to\infty}(\phi(t_0 + kT_0, 0, M_0)) = \bar{\phi}(t_0)$$

$\bar{\phi}$ is solution of (5) and $\bar{\phi}(T_0) = \bar{\phi}(0)$.

Proposition 1: For every initial condition in D, system (5) converges towards a unique T_0-periodic limit cycle.

System (1)-(4) consists of System (5) with added linear equations

$$\begin{cases} N_e\frac{d\lambda_{mes}}{d\alpha} &= \frac{1}{\tau}(\frac{M_T - M_{air}}{M_T} - \lambda_{mes}) \\ N_e\frac{d\lambda_i}{d\alpha} &= 0 \ \ \forall i \in [\ 1,\ n_{cyl}\ ] \end{cases}$$

Trivially, the λ_i are constant. On the other hand, λ_{mes} is a one dimensional asymptotically stable linear dynamics fed by a signal converging toward a limit cycle. It follows that λ_{mes} is also converging toward a limit cycle. The following proposition holds

Proposition 2: System (1)-(4) converges toward a T_0-periodic limit cycle for every initial condition in $D \times [0,1]^{n_{cyl}+1}$. This limit cycle only depends on $\lambda_1(0), \ldots, \lambda_{n_{cyl}}(0)$. We note this limit cycle

$$[0, T_0] \ni \alpha \quad \mapsto x_{\text{per}}(\alpha) \in D \times [0,1]^{n_{cyl}+1}$$

III. Observer Definition

The observer under consideration is a discrete-time Kalman filter defined around the attractive x_{per} trajectory.

A. Discrete-time reference system

We now compute a discrete approximation of System (1)-(4) by an Euler explicit scheme around the limit cycle x_{per} defined in the previous section. The sample angle is $\Delta\alpha = 6^o$ and for sake of simplicity we note $x_{\text{d}}(k) \triangleq x_{\text{per}}(k\Delta\alpha)$ and $x_{1,\text{d}}(k)$, $x_{2,\text{d}}(k)$ the first and second coordinate of $x_{\text{d}}(k)$ respectively. We define A_k, B_k and C_k as

$$A_k = \begin{bmatrix} \alpha_k & \beta_k \\ 0 & I_{n_{cyl}} \end{bmatrix} \in \mathcal{M}_{n_{cyl}+3, n_{cyl}+3}(\mathbb{R}) \qquad (6)$$

where $I_{n_{cyl}}$ is the n_{cyl}-identity matrix,

$$\alpha_k \triangleq \begin{bmatrix} 1 - \delta d'_T(x_{1,d}(k)) & 0 & 0 \\ -\delta x_{2,d}(k)p'(x_{1,d}(k)) & 1 - \delta p(x_{1,d}(k)) & 0 \\ \delta\frac{x_{2,d}(k)}{x_{1,d}(k)^2} & -\delta\frac{1}{x_{1,d}(k)} & 1 - \delta \end{bmatrix}$$

and

$$\beta_k \triangleq \begin{bmatrix} 0 & \ldots & 0 \\ \delta d_1(k\Delta\alpha) & \ldots & \delta d_{n_{cyl}}(k\Delta\alpha) \\ 0 & \ldots & 0 \end{bmatrix} \in \mathcal{M}_{3, n_{cyl}}(\mathbb{R}),$$

$$D_k \triangleq \delta \sum_{i=1}^{n_{cyl}} d_i(k\Delta\alpha) \begin{bmatrix} 1 & 1 & 0 & \ldots & 0 \end{bmatrix}^T \qquad (7)$$

and

$$C_k \triangleq \begin{bmatrix} \gamma_T & 0 & 0 & 0 & \ldots & 0 \\ 0 & 0 & 1 & 0 & \ldots & 0 \end{bmatrix} \in \mathcal{M}_{2, 3+n_{cyl}}(\mathbb{R}) \qquad (8)$$

We define the discrete-time reference dynamics as

$$\begin{cases} x_{k+1} &= A_k x_k + D_k + v_k \\ y_k &= C_k x_k + w_k \end{cases} \qquad (9)$$

where $(v, w) \in \mathbb{R}^{3+n_{cyl}} \times \mathbb{R}^2$ are added white noise. In particular, A_k, D_k and C_k are $N_0 \triangleq \frac{T_0}{\Delta\alpha}$-periodic matrices. x_k stands for the discrete time values of

$$\begin{bmatrix} M_{T,per} & M_{air,per} & \lambda_{mes,per} & \lambda_{1,per} & \ldots & \lambda_{n_{cyl},per} \end{bmatrix}$$

We note $A_* = \{A_k\}_{k\in[1,N_0]}$ and $C_* = \{C_k\}_{k\in[1,N_0]}$. Notice that $A_{k+N_0} = A_k$ and $C_{k+N_0} = C_k$.

B. Time-varying prediction algorithm

We use a time-varying Kalman predictor for estimation the individual AFR. For this purpose, we introduce the system

$$\hat{x}_{k+1/k} = A_k\hat{x}_{k/k-1} + D_k + L_k(y_k - C_k\hat{x}_{k/k-1}) \qquad (10)$$

with arbitrary chosen initial condition

$$x_{0/-1} = m_0$$

In Equation (10), L_k is the Kalman gain matrix

$$L_k = A_k P_k C_k^T (C_k P_k C_k^T + R_k)^{-1} \qquad (11)$$

The covariance error $P_k = cov(x_k - \hat{x}_{k/k-1})$ is recursively computed through the discrete periodic equation (DPRE)

$$\begin{aligned} P_{k+1} &= A_k P_k A_k^T + Q_k \\ &\quad - A_k P_k C_k^T (C_k P_k C_k^T + R_k)^{-1} C_k P_k A_k^T \end{aligned} \quad (12)$$

where $P_0 = cov(x_{0/-1})$ a freely chosen definite positive initial condition. At last, Q_k and R_k are weighting matrices, to be chosen in $\mathcal{M}_{n_{cyl}+3, n_{cyl}+3}(\mathbb{R})$ and $\mathcal{M}_{2,2}(\mathbb{R})$ respectively.

Convergence can be proven (as in [33]) using asymptotic periodicity of trajectories and a study of an approximating discrete periodic equation through uniform observability. The classic results of Bittanti [34] are at the heart of the proof.

IV. Experimental Results

A. Tests setup

The Kalman filter described above can be tested in simulation. For that purpose, a high frequency engine model was developed in AMESim [35]. The model includes a comprehensive combustion model, balance ODEs, thermal transfer laws, and gas mixing laws. The Diesel combustion model arises from Chmela's and Barba's approaches (see [36] and [37]). It is extended to multi-pulses injection, auto-ignition delay and incorporates EGR effect corrective terms [38] (see [39] for a complete description of the combustion model). To test our observer, we apply an injection duration trajectory. It produces offsets in injection which lead to AFR disturbances. More precisely, the injection steps have an effect on the average level of the measured AFR and introduce oscillations of the overall AFR signal as represented in Figure 2. These oscillations are the direct consequences of the individual AFR errors. During cylinder 1 exhaust phase, the AFR increases in the manifold, and then decreases while the other cylinders exhaust phases occur. The magnitude of the oscillations is related to the amount of the AFR differences between the cylinders and the total gas mass in the manifold (and thus to its volume). The oscillations are then propagated to the turbine, and to the UEGO sensor, where it is filtered. This is the signal that we use as an input for the Kalman filter defined in Equations (10), (11), and (12).

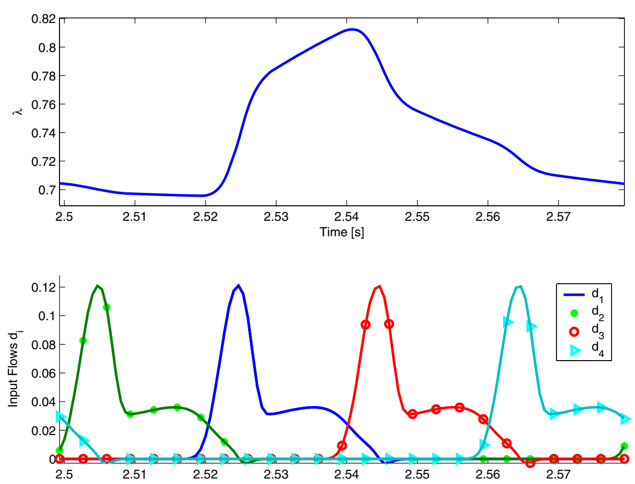

Fig. 2. AFR oscillation over 1 engine cycle during a +20% offset on cylinder 1. Top: AFR. Bottom: Cylinders output flows.

B. From simulation to experimentation

On the test bench, we use the proposed observer according to the scheme in Figure 3. Several practical issues need to be considered. We now detail these.

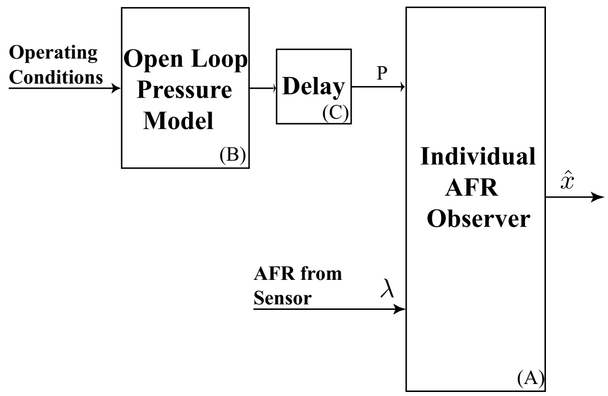

Fig. 3. Observer Scheme as used in the test bench.

1) Observer implementation: Block (A) contains the observer. The Kalman filter described in (10), (11) and (12) is extended to take into account variations of x_{per} when Ξ along varies the whole operating range in the (engine speed, load) space. Equation (10) is substituted by

$$\hat{x}_{k+1/k} = f_\Xi(\hat{x}_{k/k-1}) + D_k + L_k(y_k - C_k \hat{x}_{k/k-1}) \quad (13)$$

where the expression of A_k, D_k, C_k, L_k and P_k follow their description in Section III except α_k in (III-A) which becomes

$$\begin{bmatrix} 1 - \delta d_T'(\hat{x}_1(k), \Xi) & 0 \\ -\delta \hat{x}_2(k) p'(\hat{x}_1(k), \Xi) & 1 - \delta p(\hat{x}_1(k), \Xi) \end{bmatrix}$$

Initial conditions and (diagonal) weighting matrices (R_k and Q_k) are chosen according to preliminary simulations based on the Kalman filter presented in Section III.

2) Open loop pressure model: Exhaust pressure sensor can be expected for forthcoming HCCI vehicles only. In experimentation, we consider not having this sensor and give to the estimator an open loop value. This value is given by the open loop balance with the input flows (d_i) and output flow d_T as described previously in Section II. This model is implemented in Block (B) in Figure 3.

3) Gas transport delay: Lags due to gas transport along the engine exhaust (pipes and dead volumes), and the dead time of the sensor are not represented by the model described above in System (1), (2), and (3). Delays can be lumped into a single delay for the complete exhaust system, and the model can be inverted. This delay can be identified and kept as a constant for a given setpoint on the (engine speed, IMEP (Indicated Mean Effective Pressure)) map. This estimation is implemented in Block (C) in Figure 3.

N_e	IMEP	$100 \, \|\lambda_*\|_\infty$	$100 \, \|\lambda_*\|_{\text{mean}}$
1500	3	15.9154	6.4867
1500	6	7.6264	2.11
1500	9	11.2945	3.7399
2500	6	11.4955	3.2945
2500	9	16.1126	4.5097
3500	9	20.3286	5.5793

TABLE II

TABLE OF EXPERIMENTAL RESULTS OF THE EXTENDED KALMAN FILTER. $\|\lambda_*\|_\infty \triangleq \max_{i,\alpha} \left| \frac{\hat{\lambda}_i - \lambda_{i,ref}}{\lambda_{i,ref}} \right|$ AND $\|\lambda_*\|_{\text{MEAN}} \triangleq \text{MEAN}_{i,\alpha} \left| \frac{\hat{\lambda}_i - \lambda_{i,ref}}{\lambda_{i,ref}} \right|$

C. Experimental results

We apply the same injection duration trajectories from simulation to the test bench. The test bench under consideration is a 4 cylinders DI engine with a Variable Geometry Turbocharger (VGT) (see [39] for a complete description). Results are given in Figure 4 around an operating point (Engine Speed 1500 rpm, IMEP 9 bar). The same tuning parameters are kept from simulation to experimentation. Further, a single set of tuning parameters is kept over all operating points.

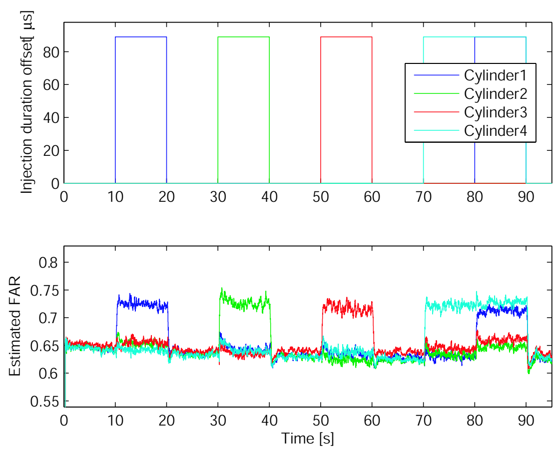

Fig. 4. Test bench results (Engine Speed 1500rpm, IMEP 9bar). Top: injection duration offsets (+20%). Bottom: estimated individual AFR

Actual FAR are not directly available but can be correlated on the experimental engine to the torque produced by each cylinder (reconstructed from the experimental individual in-cylinder pressure sensors). These correlated values, noted λ_{ref}, serve as reference for comparisons. Extensive test campaign range from 1250 rpm to 3500 rpm and from 3 to 9 bar of IMEP. Tests results are reported in Table II using two standard norms. Results appears quantitatively and qualitatively satisfactory over the considered range. Results are quantitatively and qualitatively accurate. We reproduce well the evolution of the FAR. In practice, 90% convergence is achieved within 4 engine cycles. In all test bench cases, we were able to predict the individual cylinder FAR well. Further, we can easily detect the AFR unbalance and have a good estimation of the peaks of the AFR disturbances. The magnitude of the estimated individual AFR offsets are satisfactory. Diagnosis and closed loop control strategies can be derived from this information as demonstrated in the next section.

D. Closed loop control example

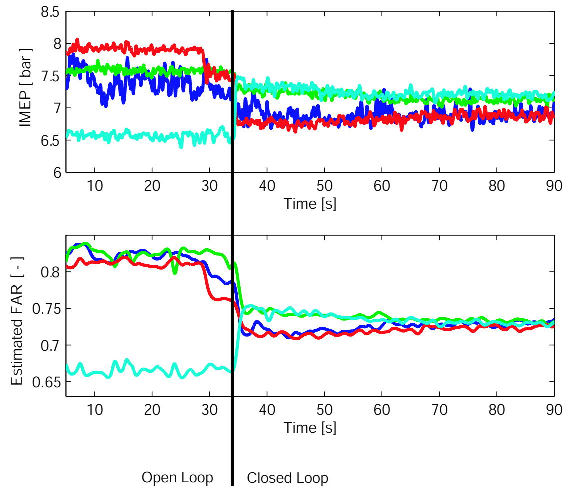

Fig. 5. Torque balancing based on individual FAR estimation: test bench results (Engine Speed 1500rpm, IMEP 7bar). We turn on the control at 34s to overcome the natural unbalance of the engine. Top: IMEP from cylinder pressure sensors. Bottom: Individual Estimated FAR with the nonlinear observer

Simple issues such as control of AFR imbalance between the cylinders can be addressed by controlling the individual injection quantities with a PI controller. Figure 5 reports the results of such a control strategy relying on the individual FAR estimation. We turn on the control at 34s and achieve tracking within a few engine cycles (10 for a 95% convergence).

V. CONCLUSIONS AND FUTURE DIRECTIONS

This paper reports the development and implementation of an individual cylinder AFR estimator. Reconstruction of the FAR from a global oxygen concentration measurement made by a *single* sensor located downstream the turbine. This information could pave the road to efficient closed loop control strategy as demonstrated on an experimental example. Its main difference with other technics proposed in the literature is that the estimation is achieved at the highest available rate: every 6^o crankshaft angle. Real-time can be achieved provided the embedded CPU can handle a $n_{cyl} + 3$ dimensional Kalman filter (typically an MPC 255 can). Availability of such an estimator giving reliable information can lead to improvements on Diesel engines in terms of combustion control, noise, and pollutant emissions.

This observer is easily transposed to various engine speeds and loads. Its dynamics are expressed in angular time scale and do not require any model for the combustion process.

Theoretically, the gains do not need to be updated when the set-point is changed. However, noise is not completely set-point independent, so in practice some re-tuning may be required. At last, we need to integrate the exhaust gas recirculation flow (EGR) in the balance equation for HCCI engines. We are currently investigating this point in a campaign on the test bench.

REFERENCES

[1] L. Guzzella and A. Amstutz. Control of Diesel engines. *Proc. in the IEEE Control Systems Magazine*, 18:53–71, 1998.

[2] U. Kiencke and L. Nielsen. *Automotive Control Systems For Engine, Driveline, and Vehicle*. SAE Internationnal, 2000.

[3] P. Gyan, S. Ginoux, J-C. Champoussin, and Y. Guezennec. Crankangle based torque estimation: Mechanistic/stochastic. In *Proc. of SAE Conference*, 2000.

[4] Y. Guezennec and P. Gyan. A novel approach to real-time estimation of the individual cylinder pressure for SI engine control. In *Proc. of SAE Conference*, 1999.

[5] J. Chauvin, G. Corde, P. Moulin, M. Castagné, N. Petit, and P. Rouchon. Real-time combustion torque estimation on a Diesel engine test bench using an adaptive Fourier basis decomposition. In *Proc. of the the* $43rd$ *IEEE Conf. Decision and Control*, 2004.

[6] J. Chauvin, G. Corde, P. Moulin, M. Castagné, N. Petit, and P. Rouchon. Real-time combustion torque estimation on a Diesel engine test bench using time-varying Kalman filtering. In *Proc. of the the* $43rd$ *IEEE Conf. Decision and Control*, 2004.

[7] J. Grizzle, K. Dobbins, and J. Cook. Individual cylinder air-fuel ratio control with a single EGO sensor. *Proc. in the IEEE Transactions on Vehicular Technology*, 40(1):357–381, February 1991.

[8] J. Chauvin, P. Moulin, G. Corde, N. Petit, and P. Rouchon. Real-time nonlinear individual cylinder Air Fuel Ratio observer on a Diesel engine test bench. In *Proc. of the IFAC World Congress*, 2005.

[9] P. Moulin, G. Corde, J. Chauvin, and M. Castagné. Cylinder individual AFR estimation based on a physical model and using Kalman filters. In *Proc. of the FISITA World Automotive Congress 2004*, number F2004V279, 2004.

[10] J Heywood. *Internal Combustion Engine Fundamentals*. McGraw-Hill, Inc, 1988.

[11] J. Kahrstedt, K. Behnk, A. Sommer, and T. Wormbs. Combustion processes to meet future emission standards. In *MotorTechnische Zeitung*, pages 1417–1423, 2003.

[12] A. Hultqvist, U. Engdar, B. Johansson, and J. Klingmann. Reacting boundary layers in a Homogeneous Charge Compression Ignition (HCCI) engine. In *Proc. of SAE Conference*, number 2001-01-1032, 2001.

[13] P. Amnéus, D. Nilsson, F. Mauss, M. Christensen, and B. Johansson. Homogeneous Charge Compression Ignition engine: Experiments and detailed kinetic calculations. In 4^{th} *International Symposium on Diagnostic and Modeling in Internal Combustion Engines*, 1998.

[14] B. Walter and B. Gatellier. Near zero NO_x emissions and high fuel efficiency diesel engine: the NADI^{TM} concept using dual mode combustion. 58(1):101–114, 2003.

[15] M. Kao and J. Moskwa. Turbocharged Diesel engine modelling for nonlinear engine control and estimation. *ASME Journal of Dynamic Systems, Measurements and Control*, 117, 1995.

[16] I. Kolmanovsky, A. Stefanopoulou, P. Moraal, and M. van Nieuwstadt. Issues in modelling and control of intake flow in variable geometry turbocharged engines. In *Proc of the* 18^{th} *IFIP Conference on System Modelling and Optimization*, 1997.

[17] C. Chiang and A. Stefanopoulou. Steady-state multiplicity and stability of thermal equilibria in Homogeneous Charge Compression Ignition (HCCI) engines. In *IEEE Proc. of 2004 Conference in Decision and Control*, 2004.

[18] M. van Nieuwstadt, I. Kolmanovsky, P. Moraal, A. Stefanopoulou, and M. Janković. Experimental comparison of EGR-VGT control schemes for a high speed Diesel engine. *Control System Magazine*, 20:63–79, 2000.

[19] M Janković and I. Kolmanovsky. Constructive Lyapounov control design for turbocharged Diesel engines. *IEEE Transactions on Control Systems Technology*, 8:288–299, 2000.

[20] M. Jung and K Glover. Comparison of uncertainty parameterisations for H-infinity robust control of turbocharged Diesel engines. 13:15–25, 2005.

[21] M. Ammann, N. Fekete, L. Guzzella, and A. Glattfelder. Model-based control of the VGT and EGR in a turbocharged common-rail Diesel engine: theory and passenger car implementation. In *Proc. of SAE Conference*, number 2003-01-0357, 2003.

[22] J. Bengtsson, P. Strandh, R. Johansson, P. Tunestål, and B. Johansson. Control of a Homogeneous Charge Compression Ignition HCCI engine dynamics. In *IEEE Proc. of 2004 American Control Conference*, 2004.

[23] P. Moraal, Y. Yacoub, U. Christen, B. Carberry, and Guérin S. Diesel particulate filter regeneration: Control or calibration? In *IFAC Symp. Advances in Automotive Control (AAC04)*, 2004.

[24] T. Auckenthaler, C. Onder, and H. Geering. Aspects of dynamic three-way catalyst behaviour including oxygen storage. In *IFAC Symp. Advances in Automotive Control (AAC04)*, 2004.

[25] T. Kreuzer, E. Lox, D. Lindner, and Leyrer J. Advanced exhaust gas aftertreatment systems for gasoline and Diesel fuelled vehicles. *Catalysis Today*, 29:17–27, 1996.

[26] J. Fantini and J.-F. Burq. Exhaust-intake manifold model for estimation of individual cylinder air fuel ratio and diagnostic of sensor-injector. In *Proc. of SAE Conference*, number 2003-01-1059, 2003.

[27] C. Carnevale and M. Hadji. Cylinder to cylinder AFR control with an asymmetrical exhaust manifold in a GDI system. In *Proc. of SAE Conference*, number 981064, 1998.

[28] A. Albrecht, J. Chauvin, S. Potteau, and G. Corde. Design of real-time torque balancing control for highly premixed combustion engine using a 1D Diesel engine model. In *Proc. of the IAV Conference "Engine process simulation and supercharging"*, 2005.

[29] J. Jensen, A. Kristensen, S. Sorensen, N. Houbak, and E. Hendricks. Mean value modeling of a small turbocharged diesel engine. In *Proc. of SAE Conference*, number 910070, 1991.

[30] P. Moraal and I. Kolmanovsky. Turbocharger modeling for automotive control applications. In *Proc. of SAE Conference*, number 1999-01-0908, 1999.

[31] P. Hartman. *Ordinary Differential Equations, Second Edition*. Birkhäuser Boston, 1982.

[32] W. Lohmiller and J.-J. Slotine. On contracting analysis for nonlinear systems. *Automatica*, 34(6):683–696, 1998.

[33] J. Chauvin, N. Petit, and P. Rouchon. Kalman filtering for real-time individual cylinder air fuel ratio observer on a Diesel engine test bench. Technical Report A/340, École des Mines de Paris, 2006.

[34] S. Bittanti, P. Colaneri, and G. De Nicolao. The difference periodic Riccati equation for the periodic prediction problem. *Proc. in the IEEE Transactions on Automatic Control*, 33(8), August 1988.

[35] IMAGINE. *AMESim user manual, http://www.amesim.com*, 2004.

[36] F. Chmela and G. Orthaber. Rate of heat release prediction for direct injection Diesel engines based on purely mixing controlled combustion. In *Proc. of SAE Conference*, number 1999-01-0186, 1999.

[37] C. Barba and C. Burkhardt. A phenomenological combustion model for heat release rate prediction in high-speed DI Diesel engines with common rail injection. In *Proc. of SAE Conference*, number 2000-01-2933, 2000.

[38] T. Jaine, A. Benkenida, P. Menegazzi, and P. Higelin. Zero dimensional computation of Diesel spray - comparison with experiments and 3D model. In *6th International Conference on Engines for Automobile*, 2003.

[39] A. Albrecht, J. Chauvin, F.-A. Lafossas, S. Potteau, and G. Corde. Development of Highly Premixed Combustion Diesel engine model : From simulation to control design. In *Proc. of SAE Conference*, number 2006-01-1072, 2006.